JOURNAL OF MATERIALS SCIENCE 28 (1993) 2227–2232

The relative residual fibre displacement after indentation loading and unloading of fibre-reinforced ceramic composites

C. H. HSUEH, M. K. FERBER, A. A. WERESZCZAK
Metals and Ceramics Division, Oak Ridge National Laboratory, Oak Ridge, TN 37831, USA

The interfacial properties of fibre-reinforced ceramic composites have been evaluated by using the indentation technique. The ratio of the residual fibre displacement after complete unloading to the fibre displacement at peak loading is examined. Assuming a constant interfacial shear stress at an unbonded interface, this ratio is 0.5. However, deviation of this ratio from 0.5 is always obtained from experimental results. Both Poisson's effect and the existence of the residual axial stress have been proposed to explain this deviation. A methodology is presented in this study to classify conditions for which either Poisson's effect or the residual axial stress dominates this deviation. The application of this methodology to Nicalon fibre-reinforced lithium aluminosilicate glass-ceramic is also illustrated.

1. Introduction

The indentation technique (Fig. 1a) has been used to evaluate the interfacial properties of fibre-reinforced ceramic composites [1, 2]. An indentor is used to push on the exposed end of an embedded fibre along the axial direction of the fibre, and forward sliding occurs at the fibre/matrix interface. The compressive loading stress, σ, increases during loading to a desired peak value, σ^*, and then decreases during unloading. Sliding occurs in the reverse sense during unloading. The stress–displacement relation at the exposed end of the fibre is recorded during the indentation loading and unloading process (Fig. 1b). This stress–displacement relation has been analysed by several researchers [1–5]. By assuming an unbonded interface and a constant interfacial shear stress along the sliding length, a simple analytical stress–displacement relation can be obtained, and the fibre displacement (at the exposed end) after complete unloading (i.e. u_0 in Fig. 1b) is half that at the peak loading stress (i.e. u^* in Fig. 1b) [1]. However, the experimental results of SiC (Nicalon) fibre-reinforced lithium aluminosilicate glass-ceramic (LAS) matrix show that u_0 is less than half of u^*, i.e. the relative residual fibre displacement, u_0/u^*, is less than 0.5 [1]. The factors contributing to u_0/u^* being less than 0.5 have been studied, and three factors have been proposed: (1) Poisson's effect [3], (2) interfacial bonding [4], and (3) residual compressive axial stresses [5].

The strength of interfacial bonding depends on the individual composite system. However, composites with relatively weak interfacial bonding, which is often needed to develop tough ceramic composites [6, 7], are considered in the present study. In this case, the contribution of the interfacial bonding strength to the negative deviation of u_0/u^* from 0.5 should be minimum. The purpose of the present study was to develop a methodology to classify conditions for which either Poisson's effect or the residual axial stress dominates the deviation of u_0/u^* from 0.5. First, the roles of Poisson's effect and of the residual axial stress on the deviation of u_0/u^* from 0.5 are summarized. Then, a methodology is developed based on the characteristics of these roles to classify conditions for which either Poisson's effect or the residual axial stress dominates the deviation of u_0/u^* from 0.5. Finally, an example of the application of the methodology to Nicalon/LAS composite is illustrated.

2. Roles of Poisson's effect and the residual axial stress on u_0/u^*

2.1. Poisson's effect

Poisson's effect is best exemplified by formulating the interfacial shear stress, τ_i, along the sliding interface. During axial loading on the fibre, the resultant interfacial radial stress consists of two components: (1) σ_c, the residual clamping stress (e.g. that due to the thermomechanical mismatch between the fibre and the matrix) which is usually considered to be a constant, and (2) σ_p, the interfacial radial compressive (or tensile) stress due to the axial compression (or tension) in the fibre and Poisson's effect. With Coulomb friction, τ_i is dictated by

$$\tau_i = \mu(\sigma_c + \sigma_p) \quad (1)$$

where μ is the coefficient of friction. The experimental evidence of Poisson's effect has been supported by results obtained from the fibre pull-out and push-out tests for SiC fibre (AVCO SCS-6)-reinforced borosilicate glass (Corning 7740). Compared to fibre pull-out, fibre push-out requires higher stress due to higher frictional resistance induced by Poisson's effect [8].

Ignoring Poisson's effect, τ_i is a constant and is equal to $\mu\sigma_c$. With Poisson's effect, τ_i is non-uniform

0022–2461

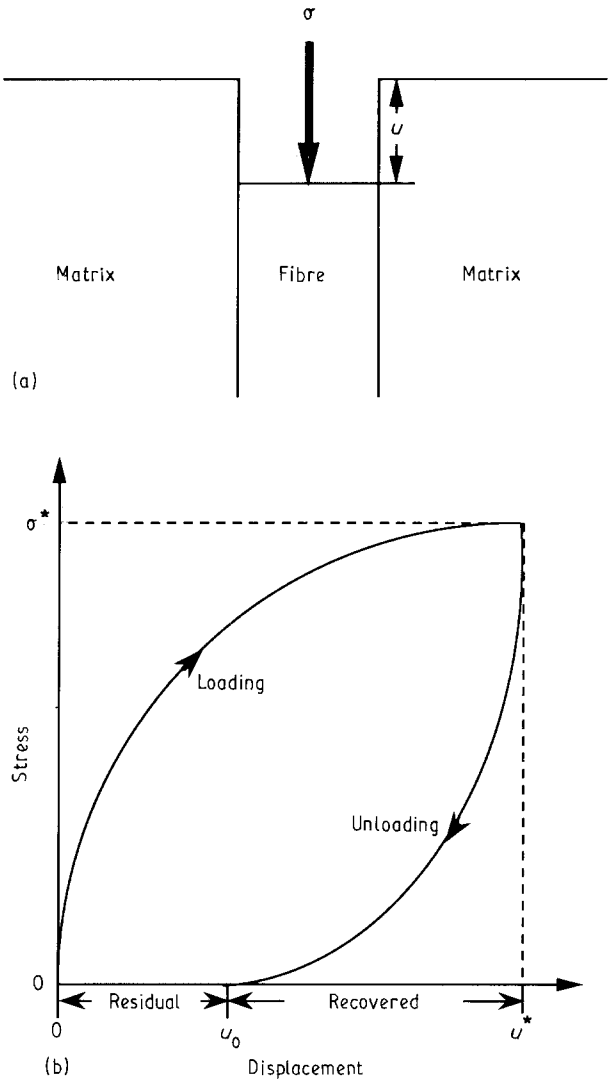

Figure 1 Schematic diagrams of (a) indentation loading showing sliding at the fibre/matrix interface and the displacement, u, at the exposed end of the embedded fibre, and (b) stress–displacement relation at the exposed end of the embedded fibre during loading and unloading.

due to the variation of σ_p along the sliding length. For example, during indentation loading, the axial compressive stress in the fibre and, hence, the interfacial shear stress decrease with increasing distance underneath the loaded surface, because of the stress transfer from the fibre to the matrix through interfacial shear [3].

The stress analysis considering Poisson's effect is very complicated. However, schematic examples of the axial strain distributions in the fibre, ε, at peak loading and complete unloading are shown in Fig. 2a, and b (see Fig. 2b in [3] for further detail), respectively. The slope of the curve is dictated by the stress transfer equation, such that [1–5]

$$\frac{d\varepsilon}{dz} = -\frac{2\tau_i}{aE_f} \tag{2}$$

where z is the axial coordinate, a and E_f are the radius and Young's modulus of the fibre, respectively. The non-linearity of the curve is due to Poisson's effect. The axial strain at the exposed end of the fibre is ε^* at the peak loading, and returns to zero after complete unloading. The axial displacement at the exposed end of the fibre is the area encompassed by the axial strain curve and the z-axis, and is represented by the shaded area in Fig. 2. The relative residual fibre displacement, u_0/u^*, being less than 0.5 can be visualized in Fig. 2b. The importance of Poisson's effect can be seen by comparing σ_c with σ_p. Poisson's effect becomes more prominent when Poisson's ratio of the fibre or the ratio of the loading stress to the residual clamping stress increases [3].

2.2. The residual axial stress

In the presence of the residual axial stress, the relative residual fibre displacement has previously been analysed by ignoring Poisson's effect [5]. Schematic diagrams of the axial strain distributions in the fibre, ε, before loading, at peak loading, and after complete unloading are shown in Fig. 3a–c, respectively. The residual compressive axial strain is zero at the surface, and increases linearly to a constant, ε_z (see Fig. 3a), with the slope given by Equation 2, in which τ_i is assumed to be a constant. Displacements at the exposed end of the fibre are represented by the shaded areas in Fig. 3b for peak loading, and in Fig. 3c after complete unloading.

Simple analytical solutions are obtained for the stress–displacement relations, and the relative residual displacement, u_0/u^*, after complete unloading is [5]

$$\frac{u_0}{u^*} = 0 \quad \text{for } (\sigma^* < 2\sigma_z) \tag{3a}$$

$$\frac{u_0}{u^*} = 1 - \frac{1}{2\left[1 - 2\left(\frac{\sigma_z}{\sigma^*}\right) + 2\left(\frac{\sigma_z}{\sigma^*}\right)^2\right]}$$

$$\text{for } (\sigma^* > 2\sigma_z) \tag{3b}$$

where σ_z is the residual compressive axial stress ($= E_f\varepsilon_z$) in the fibre. The existence of the residual compressive axial stress results in u_0/u^* being less than 0.5 (Fig. 3c). Conversely, in the presence of the residual tensile axial stress, u_0/u^* is greater than 0.5. However, the effect of the residual axial stress on the deviation of u_0/u^* from 0.5 becomes less prominent when the peak loading stress on the fibre increases [5].

3. The methodology

The methodology can be established based on the opposite trends of the roles of the Poisson's effect and of the residual axial stress on the deviation of the relative residual fibre displacement, u_0/u^*, from 0.5 when the peak loading stress, σ^*, on the fibre increases. Experimental results of increasing negative deviation of u_0/u^* from 0.5 with increasing σ^* would indicate that this deviation is dominated by Poisson's effect based on the last section. On the contrary, experimental results of decreasing negative deviation of u_0/u^* from 0.5 with increasing σ^* would indicate that this deviation is dominated by the residual axial stress.

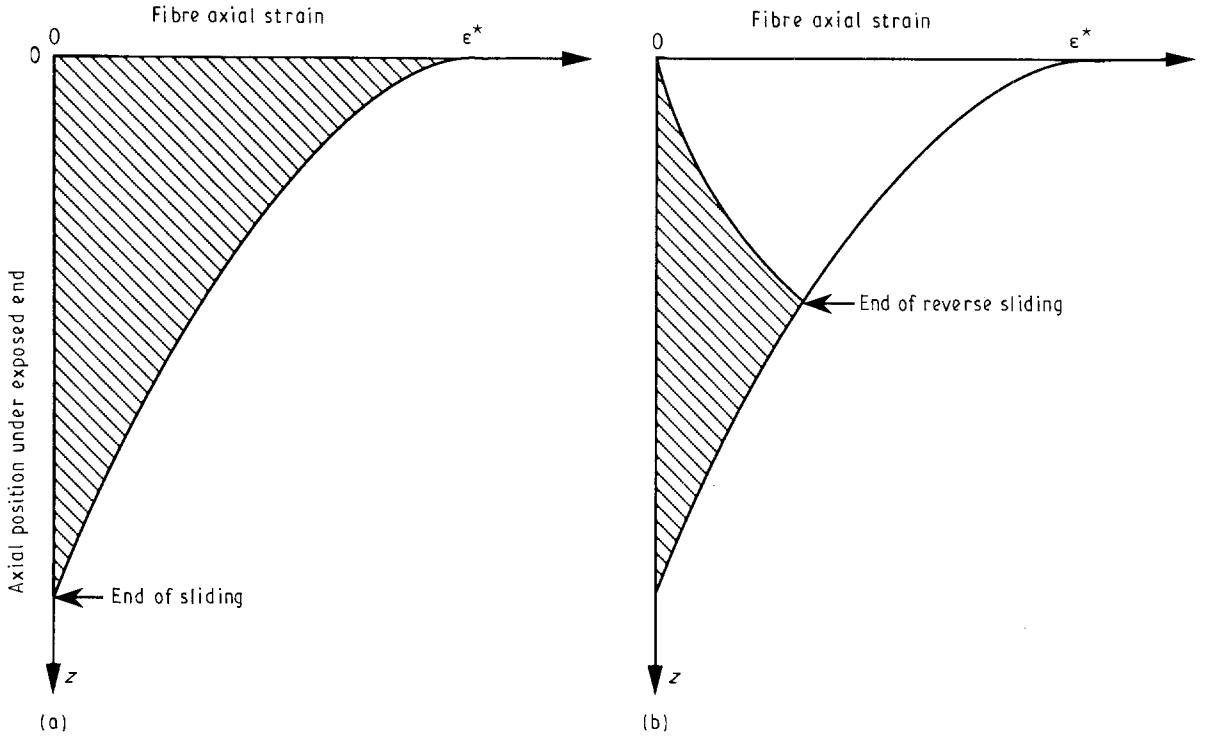

Figure 2 Schematic illustration of the axial strain distribution in the fibre, ε, (a) at peak loading, and (b) after complete unloading when Poisson's effect is considered. Displacements at the exposed end of the fibre are represented by the shaded areas.

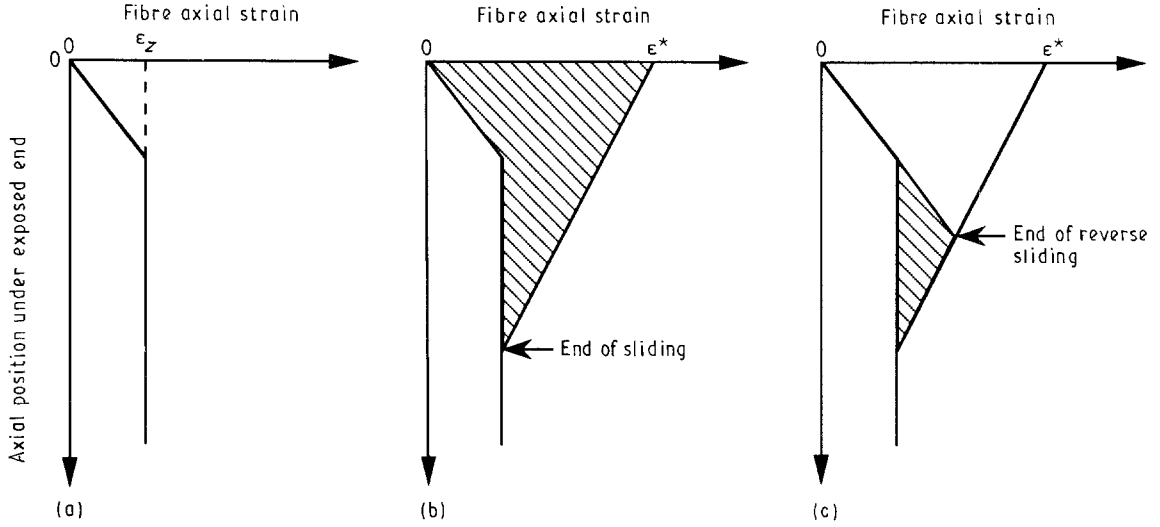

Figure 3 Schematic illustration showing the axial strain distribution in the fibre (a) before loading, (b) at peak loading, and (c) after complete unloading when the residual axial stress, σ_z ($= E_f\varepsilon_z$), is considered (for $\varepsilon^* > 2\varepsilon_z$). Displacements at the exposed end of the fibre are represented by the shaded areas.

4. The application of the methodology

To test the methodology, experiments were performed on Nicalon/LAS composites, which have weak bonding at the interface and $E_f = 200$ GPa, $E_m = 80$ GPa, $\nu_f = 0.15$ and $\nu_m = 0.3$, where E and ν are Young's modulus and Poisson's ratio, and the subscripts f and m denote the fibre and the matrix, respectively. The volume fraction of fibres in the composite is 0.3. Owing to this high volume fraction, the rule of mixtures is used to estimate the elastic properties for the matrix (i.e. $E_m = 116$ GPa, and $\nu_m = 0.25$) because the material surrounding the fibre is treated as the matrix in analysing the indentation test [3].

4.1. Experiments

The experimental procedures in obtaining the relative residual fibre displacement, u_0/u^*, versus the peak loading stress, σ^*, are summarized as follows. First, indentation loading and unloading was performed on Nicalon/LAS composites at different maximum loading stresses, σ^*, and both the maximum fibre displacement, u^*, at peak loading and the residual fibre displacement, u_0, after complete unloading were recorded. Then, a second order polynomial was fitted to the u^* versus σ^* and the u_0 versus σ^* curves, respectively, as shown in Fig. 4. Finally, the resulting polynomial expressions were used to calculate u_0/u^* as a function of σ^* (see Fig. 5).

4.2. Predictions

The predicted results for the analysis considering Poisson's effect [3] were calculated using $\mu = 0.089$

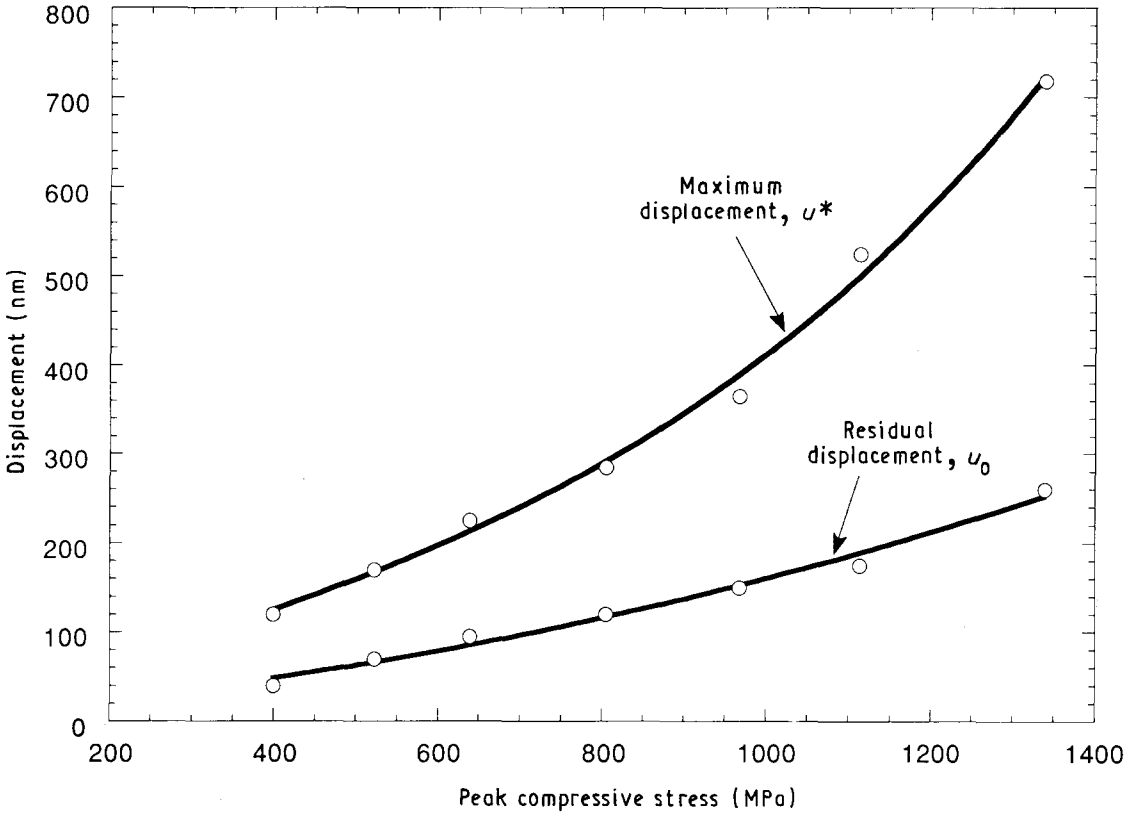

Figure 4 The maximum fibre displacement, u^*, at peak loading, and the residual fibre displacement, u_0, after complete unloading, as functions of the peak loading stress, σ^*, for Nicalon/LAS composites. Second-order polynomial fitting curves (——) are also shown.

and $\sigma_c = -21$ MPa (negative sign for compression), which have been obtained previously [3] by applying the analysis to the Nicalon/LAS composite. However, to illustrate the trend of Poisson's effect, the predicted results for $\nu_f = 0.3$ (other than 0.15) were also shown.

The prediction of u_0/u^* from the analysis considering the residual axial stress (i.e. Equation 3b) [5] is contingent upon the determination of the residual axial stress, σ_z. Ideally, σ_z can be obtained from extrapolation of the experimental u_0/u^* versus σ^* curve (i.e. $u_0 = 0$ at $\sigma^* = 2\sigma_z$). However, it is not feasible in the present study because a significant error in estimating σ_z can result from extrapolation of the limited data available at low peak loading stresses. Alternatively, σ_z can be obtained from the residual stress analysis. When the residual stress is due to an isotropic mismatch strain between the fibre and the matrix, the residual axial stress in the fibre can be related to the residual radial stress at the bonded fibre/matrix interface by combining Equations 7a and b in [9], such that

$$\sigma_z = \left[1 + \frac{(1 + \nu_m)E_f}{(1 + \nu_f)E_m}\right]\sigma_c \qquad (4)$$

The residual axial stress estimated from Equation 4 and $\sigma_c = -21$ MPa is -60 MPa.

Using $\sigma_z = -60$ MPa, the predicted results for the analysis considering the residual axial stress are shown in Fig. 5. To illustrate the effect of σ_z, the predicted results for $\sigma_z = -30$ MPa are also shown.

4.3. Comparison

The predictions based on Poisson's effect consideration and the residual axial stress consideration have the opposing trends of the peak loading stress dependence of u_0/u^* (Fig. 5). Considering the curves predicted for $\sigma_z = -60$ MPa from Equation 3b and for $\nu_f = 0.15$ based on Poisson's effect, it is evident that for $-\sigma^* < 700$ MPa, the residual axial stress dominates the relative residual displacement. This domination is reflected by the deviation of the predicted u_0/u^* from the idealized value of 0.5 based on the residual axial stress consideration, is greater than that based on Poisson's effect. As $-\sigma^*$ exceeds 700 MPa, u_0/u^* is controlled by Poisson's effect. A similar opposing trend is exhibited by the experimental data, which are well-described by Equation 3b for $-\sigma^* < 700$ MPa and by Poisson's effect for $-\sigma^* > 700$ MPa.

The predicted curves in Fig. 5 also illustrate the effects of the magnitudes σ_z and ν_f on the relative residual fibre displacement. Considering the effect of the residual axial stress, a decrease (in magnitude) in σ_z shifts the u_0/u^* versus σ^* curve to the left which, in turn, lowers the critical transition stress from 700 MPa to 500 MPa. Considering Poisson's effect, an increase in ν_f increases the extent of the Poisson's effect, and the transition stress is lowered to approximately 550 MPa.

4.4. Discussion

The opposing effects of σ_z and ν_f on the predicted u_0/u^* versus σ^* curves are confirmed by the experimental results (Fig. 5). However, a more accurate estimation of σ_z and ν_f with the above methodology is limited by several factors. First, Poisson's effect and the residual axial stress effect are treated separately in

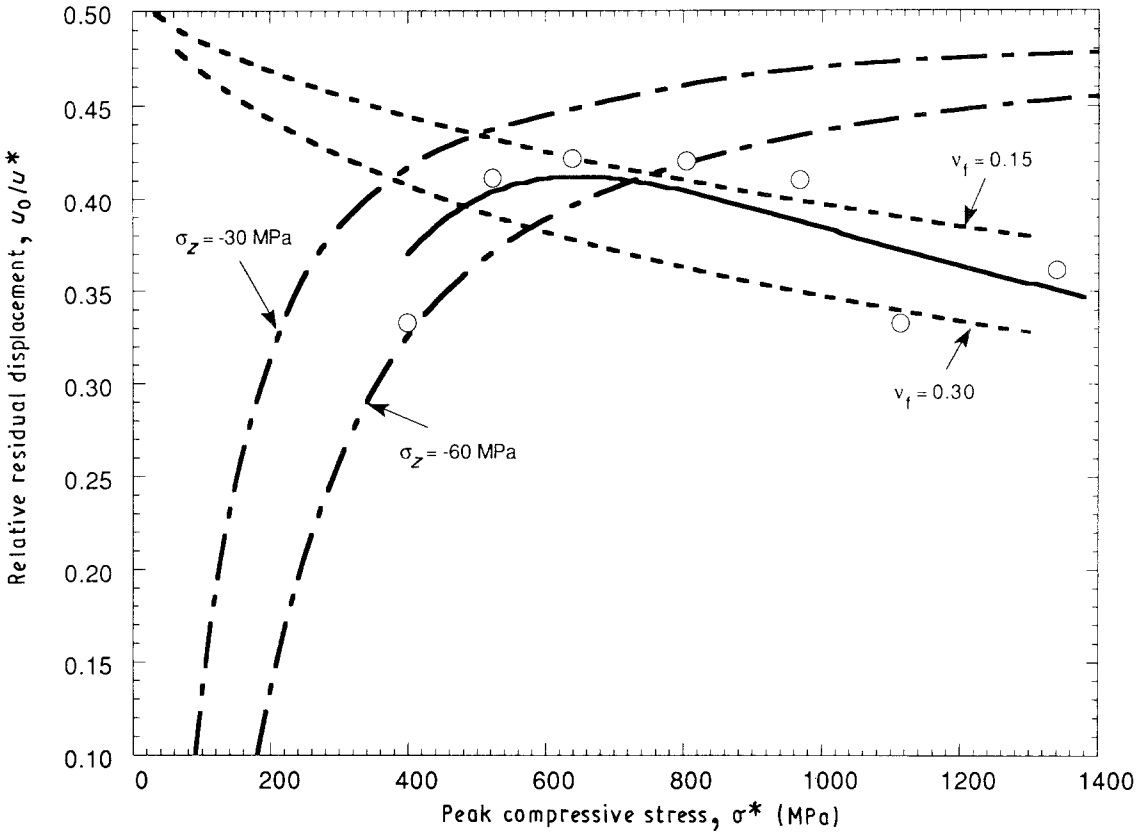

Figure 5 The relative residual fibre displacements after indentation loading and unloading, u_0/u^*, as functions of the peak loading stess, σ^*. (– – –) Poisson's effect consideration, (— · —) residual axial stress consideration, (○) experimental data, (——) second-order polynomial fitting for Nicalon/LAS composites.

the present study, and possible synergistic effects are not taken into account. Second, the influence of interfacial bonding upon the relative residual axial displacement is ignored. Available experimental data for the Nicalon/LAS system indicate that a small but finite loading stress (< 50 MPa) is generally required to initiate fibre sliding. Consequently, the accurate evaluation of σ_z and v_f from the experimental u_0/u^* versus σ^* data awaits development of a more comprehensive model accounting for these three factors: Poisson's effect, residual axial stresses, and interfacial bonding.

5. Conclusion

Assuming a constant interfacial shear stress along the sliding interface (i.e. ignoring Poisson's effect), the analytical solution for indentation loading and unloading can be readily obtained [1, 5]. Considering Poisson's effect, the stress analysis is complicated, and existing solutions consider only the bonding and the residual clamping stress at the interface but not the residual axial stress [3, 4]. A complete solution accounting for the residual axial stress can be obtained by modifying the analyses given elsewhere [3, 4] based on other work [10, 11]; however, the analyses are formidable and are beyond the scope of the present study.

In the present study, a methodology is presented to classify conditions for which either Poisson's effect or the residual axial stress dominates the deviation of the relative residual fibre displacement from 0.5. The general trend shows that Poisson's effect becomes more important when the peak loading stress to the residual clamping stress ratio increases, and that the effect of the residual axial stress becomes more important when the peak loading stress to the residual axial stress ratio decreases. However, in the presence of both a weak interface and a strong residual axial stress, interfacial debonding and relaxation of the residual axial stress can occur without external applied stresses [11]. Protrusion of the fibre from the composite during specimen preparation has been observed for the Nicalon fibre reinforced-macro defect-free cement composite [2] which indicates existence of both weak interfaces and residual compressive axial stresses in the fibre. Compared to Poisson's effect, the effect of the residual axial stress on the deviation of the relative residual fibre displacement from 0.5 after indentation loading and unloading tends to be obscured for the ceramic composite due to the weak interface.

Acknowledgements

The authors thank Drs P. F. Becher, A. Bleier and W. C. Oliver for reviewing the manuscript. This research was jointly sponsored by the US Department of Energy, Division of Materials Sciences, and Assistant Secretary for Conservation and Renewable Energy, Office of Industrial Technologies, Industrial Energy Efficiency Division, under contract DE-AC05-84OR21400 with Martin Marietta Energy Systems, Inc.

References

1. D. B. MARSHALL and W. C. OLIVER, *J. Amer. Ceram. Soc.* **70** (1987) 542.
2. M. K. FERBER, A. A. WERESZCZAK, D. H. HASEN and J. HOMENY, *Compos. Sci. Technol.*, in press.
3. C. H. HSUEH, M. K. FERBER and P. F. BECHER, *J. Mater. Res.* **4** (1989) 1529.
4. C. H. HSUEH, *J. Mater. Sci.* **25** (1990) 4080.
5. D. B. MARSHALL and W. C. OLIVER, *Mater. Sci. Engng* **A126** (1990) 95.
6. A. G. EVANS and R. M. McMEEKING, *Acta Metall.* **34** (1986) 2435.
7. P. F. BECHER, C. H. HSUEH, P. ANGELINI and T. N. TIEGS, *J. Amer. Ceram. Soc.* **71** (1988) 1050.
8. C. H. HSUEH, J. D. BRIGHT and D. K. SHETTY, *J. Mater. Sci. Lett.* **10** (1991) 135.
9. C. H. HSUEH, P. F. BECHER and P. ANGELINI, *J. Amer. Ceram. Soc.* **71** (1988) 929.
10. C. H. HSUEH, *Mater. Sci. Engng* **A145** (1991) 135.
11. *idem, ibid.* **A145** (1991) 143.

Received 18 March
and accepted 12 October 1992